Journal of Biomolecular Screening
2016, Vol. 21(9) 931–941

DOI: 10.1177/1087057116650965
jbx.sagepub.com
SAGE

Assay Establishment and Validation of a High-Throughput Screening Platform for Three-Dimensional Patient-Derived Colon Cancer Organoid Cultures

Karsten Boehnke[1], Philip W. Iversen[2], Dirk Schumacher[3,4], María José Lallena[1], Rubén Haro[5], Joaquín Amat[1], Johannes Haybaeck[6], Sandra Liebs[4,7], Martin Lange[8], Reinhold Schäfer[3,4], Christian R. A. Regenbrecht[3,9], Christoph Reinhard[10,*], and Juan A. Velasco[1,*]

Abstract

The application of patient-derived three-dimensional culture systems as disease-specific drug sensitivity models has enormous potential to connect compound screening and clinical trials. However, the implementation of complex cell-based assay systems in drug discovery requires reliable and robust screening platforms. Here we describe the establishment of an automated platform in 384-well format for three-dimensional organoid cultures derived from colon cancer patients. Single cells were embedded in an extracellular matrix by an automated workflow and subsequently self-organized into organoid structures within 4 days of culture before being exposed to compound treatment. We performed validation of assay robustness and reproducibility via plate uniformity and replicate-experiment studies. After assay optimization, the patient-derived organoid platform passed all relevant validation criteria. In addition, we introduced a streamlined plate uniformity study to evaluate patient-derived colon cancer samples from different donors. Our results demonstrate the feasibility of using patient-derived tumor samples for high-throughput assays and their integration as disease-specific models in drug discovery.

Keywords

cell-based assays, oncology, assay validation, patient-derived organoid culture

Introduction

High-throughput cancer cell line screening assays are fundamental tools to evaluate drug sensitivity patterns and pharmacogenomic profiling that may guide early-phase clinical trials of novel agents and rational cancer therapeutic strategies.[1] Traditional two-dimensional (2D) cell-based assays are commonly employed to determine the potency of active lead molecules; however, their value in predicting clinical response to novel agents is limited. In recent years, the importance of the tumor microenvironment and the three-dimensional (3D) aspects of solid tumors have promoted strong interest in more precisely mimicking tumor cell growth in vitro.[2] Consequently, novel complex 3D culture systems and more sophisticated xenograft models are currently reinvigorating translational research efforts and predictive biomarker development studies.[3–8]

Recently, Sato and colleagues[9] succeeded in discovering the growth conditions for mouse intestinal cells that self-organize into so-called organoid cultures. Organoids are developed by seeding dissociated tissue-derived cells into a 3D semisolid extracellular matrix and expanding these cells in defined medium.[9,10] The methodology was subsequently

[1]Eli Lilly and Company, Lilly Research Laboratories, Quantitative Biology, Alcobendas, Madrid, Spain
[2]Eli Lilly and Company, Lilly Research Laboratories, Global Discovery Statistics, Lilly Corporate Center, Indianapolis, IN, USA
[3]Institute of Pathology, Charité-Universitätsmedizin Berlin, Berlin, Germany
[4]German Cancer Consortium (DKTK), German Cancer Research Center (DKFZ), Heidelberg, Germany
[5]Eli Lilly and Company, Lilly Research Laboratories, Discovery Chemistry Research & Technologies, Alcobendas, Madrid, Spain
[6]Institute of Pathology, Medical University Graz, Graz, Austria
[7]Charité Comprehensive Cancer Center, Charité-Universitätsmedizin Berlin, Berlin, Germany
[8]Bayer Pharma AG, Berlin, Germany
[9]CPO - Cellular Phenomics & Oncology, Berlin-Buch GmbH, Berlin, Germany
[10]Eli Lilly and Company, Lilly Research Laboratories, Oncology Translational Research, Lilly Corporate Center, Indianapolis, IN, USA
*These authors jointly directed this work.

Received Mar 28, 2016, and in revised form Apr 26, 2016, Accepted for publication Apr 27, 2016.

Supplementary material for this article is available on the *Journal of Biomolecular Screening* Web site at http://jbx.sagepub.com/supplemental.

Corresponding Author:
Juan A. Velasco, Eli Lilly and Company, Lilly Research Laboratories, Quantitative Biology, Alcobendas, Madrid, Spain.
Email: jvelasco@lilly.com

refined to establish human organoid cultures for different tumor entities.[10–13] Furthermore, the possibility of expansion and storage of an organoid biobank enables the long-term use of patient-derived organoid cultures as experimental tools in basic and clinical research.[14] The application of these physiologically relevant cultures as a new generation of test platforms for future drug discovery efforts could bridge the gap between primary 2D cell-based screening and animal and human trials.[15,16] However, the implementation of novel cell-based assay systems to promote a successful development and selection of active compound leads requires reliable and robust test platforms.

Here we apply patient-derived 3D (PD3D) colon cancer organoid samples as 384-well–based cultures to examine whether in vitro assays that comprise primary patient-derived tumor material would be amenable for an automated liquid-handling platform. We focused our study on the validation of assay robustness and reproducibility by running plate uniformity and replicate-experiment studies. In addition, we used various patient-derived colon cancer culture strains to validate the assay conditions and performance on a different organoid sample set.

Materials and Methods

Human Primary and Metastatic Colon Cancer Tissues

All tumors were obtained from patients with high-grade colon carcinoma at clinical centers in Germany (Charité Universitätsmedizin Berlin–Campus Benjamin Franklin, Berlin) and Austria (Medical University of Graz, MUG, Graz) under the regulations of the respective ethical boards. Resident pathologists inspected and classified all resected colon carcinoma tissues. The following patient-derived samples (based on the OncoTrack ID system) were used for this study: 159-MB-P-TF-01-03, 250-MW-P-TF-01-03, 327-MB-P-TF-01-03, and 364-CB-M-MF-01-04.

Generation and Propagation of Patient-Derived Organoid Cell Cultures

Upon receipt of resected colon carcinomas, fatty and necrotic tissue was removed macroscopically. Tumor tissue was rinsed with Hank's Balanced Salt Solution (Gibco), manually minced using sterile scalpels, and digested in Advanced DMEM/F12 (Gibco) supplemented with 1x P/S, collagenase IV (Sigma-Aldrich), DNaseI (AppliChem), Dispase (StemCell Technologies), and amphotericin B (Sigma-Aldrich) at 37 °C for 60 min. During incubation, the tissue fragments were repeatedly suspended with a 10 mL pipette. The digestion was stopped after 1 h by pelleting the suspension at 300*g* for 3 min and resuspension in Advanced DMEM/F12, supplemented with 1x penicillin/streptomycin (P/S). To exclude crude undigested tissue fragments but retain multicellular aggregates,[17] the suspension was filtered through a 100 µm cell strainer (Corning). The flow-through was subjected to consecutive filtration using a 40 µm cell strainer. Retained cell aggregates were recovered by rinsing with 10 mL Advanced DMEM/F12 and transferred into a Petri dish. The 40 to 100 µm aggregates and <40 µm flow-through were centrifuged at 300*g* for 3 min. After depletion of red blood cells using Red Blood Cell Lysis Solution (Miltenyi) and a final pelleting step, both fractions were separately mixed with phenol-red free, growth factor–reduced Matrigel (Corning) and seeded into 24-well plates in 20 µL aliquots. Solidified droplets were carefully overlaid with 500 µL of culture medium (Advanced DMEM supplemented with 1x GlutaMAX, 1x P/S, 10 mM HEPES buffer, 1x N2 Supplement, 1x B27 Supplement [all Gibco], 1 mM N-Acetyl-L-cysteine [Sigma-Aldrich], 20 ng/mL basic fibroblast growth factor [New England Biolabs], and 50 ng/mL epidermal growth factor [Sigma]) according to published protocols.[10] During the first week, 1.25 µg/mL amphotericin B and 10 µM ROCK-II inhibitor Y27632 (Sigma-Aldrich) were added to cultures. The cultures were passaged when the aggregates reached a diameter of approximately 800 µm. Cellular aggregates were released from Matrigel by adding 5 mL Advanced DMEM/F12 and centrifugation. Pellets were digested with TrypLE (Gibco). Trypsinization was stopped with 5 mL Advanced DMEM/F12, and digested cell clusters were replated on a 12-well plate.

Microscopy Analysis

For immunofluorescence imaging, patient-derived organoid cultures were fixed with 4% paraformaldehyde and permeabilized with 0.05% Tween-20 for 30 min. The samples were then washed in phosphate-buffered saline (PBS) with 7.5% bovine serum albumin (BSA). F-actin was stained accordingly with TRITC-labeled phalloidin (Sigma Aldrich). Anti-Ki-67 conjugated to Alexa Fluor 488 (Abcam) was incubated at 4 °C for 24 h and removed by washing with PBS with 7.5% BSA. Nuclei were stained with DAPI (Sigma Aldrich) for 30 min; residual DAPI was washed off with PBS. For image analysis, PBS was removed from wells and mounting medium was added. Microscopy was performed with a Zeiss Axiovert 400 microscope.

For the time-lapse analysis, the growth of the organoid cultures in 384-well plates was monitored using an HC PL APO 10X/0.40 AN (10×) objective, a Hamamatsu ORCA-AG CCD camera, and an inverted motorized microscope (Leica DMI 6000B) coupled with an incubation system to control the temperature and CO_2 levels during the course of the experiments. Images were taken every 15 min for 72 h using Leica LAS AF software (version 2.4.1). Confocal microscopy was carried out using a Leica TCS SP5 X confocal microscope equipped with a resonant scanner, a dry 20× Plan Apochromatic, 0.7 AN objective, and Leica LAS

AF software (version 2.4.1) for image capturing and the Imaris software (Bitplane) for image analysis.

Semiautomated High-Throughput Drug Response Assays

Organoid cultures were digested with TrypLE (Gibco) until a single-cell suspension was achieved. Disaggregation was stopped with Advanced DMEM/F12, and cells were counted. Suspended in growth factor–reduced Matrigel (Corning), 5000 cells per well were seeded into 384-well plates using a robotic platform (Tecan Freedom EVO MCA 96; **Suppl. Fig. S1**). For the seeding process, the plates were located on a rack cooled (–5 °C) by a minichiller (Huber). Cells were precultured for 4 d prior to compound treatment, and the plates were sealed with Breathe-Easy sealing membrane (Sigma) during the whole culture period. The treatment duration was assessed by the doubling time for each cell culture strain. The population doubling time was determined by analyzing the cell viability of consecutive culture days to generate a growth curve. The CellTiter-Glo (Promega) cell viability assay was used to measure cell viability by luminescence measurement of adenosine triphosphate (ATP) consumption. The ATP reagent was added to each well of a 384-well plate, and the intensity of luminescence was measured using the EnVision plate reader (PerkinElmer) 30 min after the addition of the reagent. For the plate uniformity studies, 5 μM staurosporine was used as the reference compound for the Min (minimum signal) wells. The Max (maximum signal) wells were cultured with the vehicle control (0.25% DMSO). For the concentration-response curves (CRCs), staurosporine was used with 10 concentrations ranging from 5 μM to 0.25 nM with 1:3 serial dilution steps (**Suppl. Fig. S2**) using Tecan Freedom EVO MCA 384. Subsequently, the compound dilution plate was stamped onto the cell assay plate using Tecan Freedom EVO MCA 384. To measure cell viability, the percentage of activity or inhibition was calculated as follows:

$$\%\,activity = \frac{signal - AVG_{\min}}{AVG_{\max} - AVG_{\min}} * 100.$$

Being,

$$\%\,inhibition = 100 - \%\,activity.$$

To obtain IC_{50} values, the four-parameter nonlinear logistic equation (four-parameter logistic CRC) was used:

$$y = bottom + \frac{(top - bottom)}{1 + \left(\frac{x}{IC_{50}}\right)^{slope}}.$$

Results

Establishment of Patient-Derived Colon Cancer Organoid Cultures in 384-Well Format

Primary patient-derived colon cancer samples were cultured and expanded as 3D organoid models in Matrigel droplets in a 12-well format as previously described.[14] During the culture period, small organoids developed into more complex and larger organoids characterized by numerous budding structures (**Fig. 1A**, **B**). Notably, even complex organoid structures showed structural integrity and Ki-67–positive cells at the outer surface indicating sustained growth and regular morphogenesis during long-term culture (**Fig. 1C**, **D**). To determine whether patient-derived cells could be seeded and subsequently cultured as organoid structures in 384-well format, we aimed at establishing a workflow that entails controlled assay starting conditions with automated liquid-handling platforms (**Fig. 1E**; **Suppl. Fig. S1**). PD3D organoid structures were disaggregated into single-cell suspension to allow for cell number measurement. To avoid Matrigel solidification, the single-cell suspension was seeded into the 384-wells by an automated platform in chilling conditions (**Suppl. Fig. S1**). Importantly, the process allowed for a uniform distribution of the single cells suspended in Matrigel (**Fig. 1F**, **G**). During the preculture period of 4 d, single cells formed complex structures indicating a progressive morphogenesis into 3D constructs in 384-well format (**Fig. 1H**, **I**). To examine whether the tissue architecture of these 3D constructs could be considered as organoid-like structures, we performed confocal imaging analysis (**Fig. 1J–M**). Strikingly, the cultures featured a polarized epithelium with a central cell-free lumen and Ki-67–positive cells at the surface (**Fig. 1K–M**). These results suggest that single cells could be cultured within Matrigel in 384-well plates and displayed regular organoid-like morphogenesis.

Spatial Uniformity Assessment of 384-Well Based Organoid Cultures

Given the well-known probability of plate edge or side effects in high-throughput cell-based assay formats due to evaporation during long incubation periods, there has been much interest in developing statistical tools and optimizing the experimental conditions to correct these types of systemic errors.[18,19] To evaluate the edge and drift effects in our patient-derived organoid assay, we precultured 384-well plates and added medium containing 0.25% DMSO (vehicle control) at day 4 into all wells. Upon additional 4 d in culture, the plates were analyzed by luminescence measurement of ATP consumption, and the values for the relative luminescence units (RLU) were visualized with the well-level location (**Fig. 2**). We observed irregular spatial distribution of luminescence/RLU(s) throughout the plate with high values located at the outer wells in the columns 1 and 24 and in the rows A and P

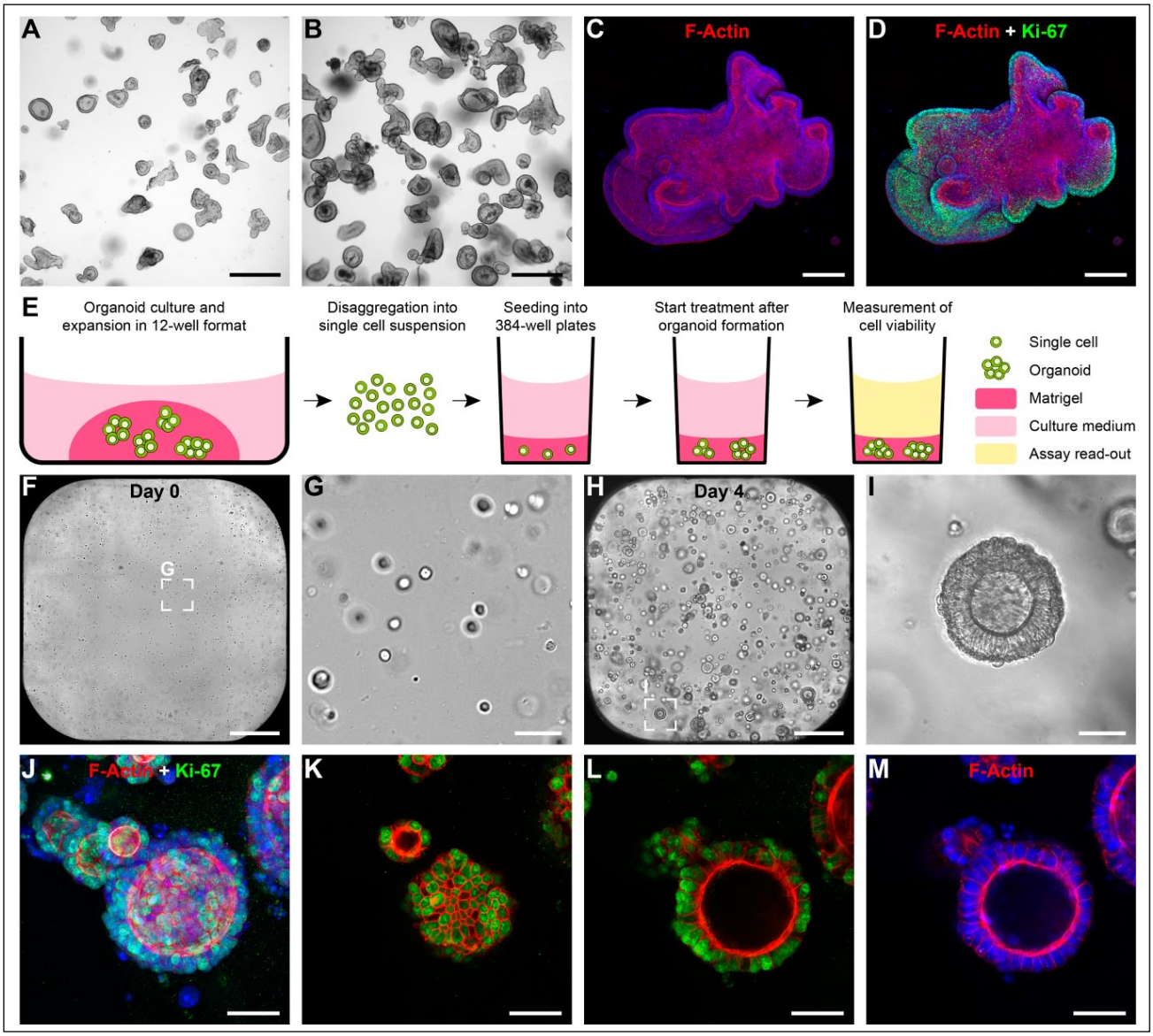

Figure 1. Establishment of patient-derived organoid cultures in 384-well format. (**A, B**) Patient-derived organoid samples were cultured and expanded (4 d in culture in **A** and 12 d in culture in **B**) in Matrigel droplets in 12-well plates. (**C, D**) Long-term cultures were stained for F-actin (phalloidin, red), Ki-67 (green), and DAPI (blue) and exhibited numerous budding structures, morphological integrity, and Ki-67–positive cells at the organoid surface. (**E**) Organoid samples were disaggregated into single-cell suspension and were seeded into 384-well plates. Compound treatment was initiated after a preculture period of 4 d, and cell viability was analyzed after a culture period covering two population doubling times. (**F–I**) Single cells were seeded into 384-well plates and subsequently formed three-dimensional organoid structures within 4 d of preculture. (**J–M**) Confocal image analysis of patient-derived organoid cultures in 384-well format stained for F-actin (phalloidin, red), Ki-67 (green), and DAPI (blue) illustrates the maximum intensity projection (**J**), an optical section of the surface (**K**), and the DAPI-negative luminal compartment of the center (**L**, **M**) of an organoid structure. Scale bars: A, B, F, H = 500 µm; C, D = 200 µm; G, I–M = 50 µm.

(**Fig. 2A**, **B**). Sealing membranes for multiwell plates are designed to allow effective gas exchange while reducing evaporation. To reduce these well-to-well variations, we tested sealing membranes covering the 384-well plates for defined culture periods. First, we employed the sealing membrane after the preculture period when the vehicle control was added to the plates. We observed a slight reduction of the irregular spatial distribution; however, higher values could still be detected at the corners of the plates (**Fig. 2C**, **D**). In contrast, when the sealing membranes were used throughout the whole incubation time, including both the preculture period and the treatment period, the RLU values were evenly distributed with no signs of drift or edge effects (**Fig. 2E**, **F**). These changes reduced the coefficient of variation (CV)

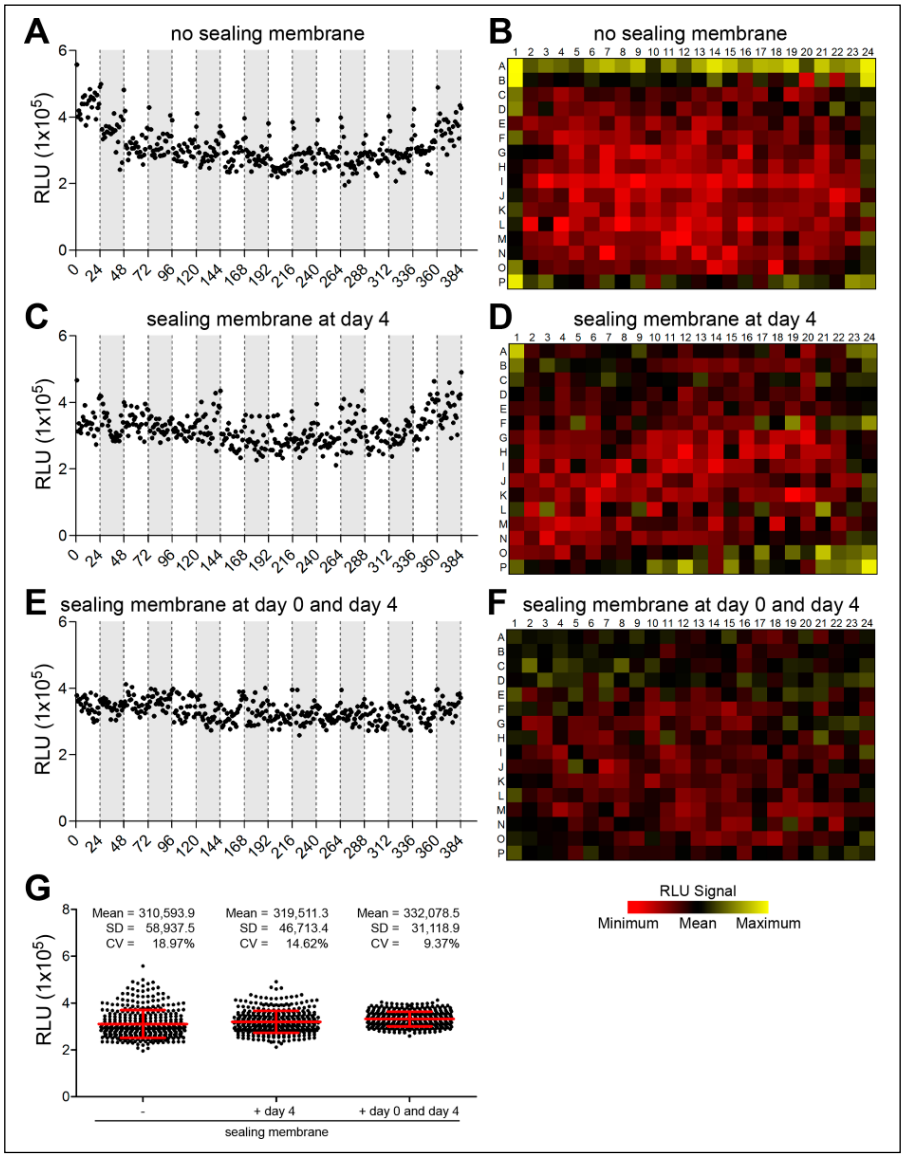

Figure 2. Spatial uniformity assessment with optimized assay conditions. Patient-derived organoid samples in 384-well format were precultured for 4 d and subsequently treated with the vehicle control. (**A, B, G**). When plates were incubated without sealing membranes, plate edge effects were detected by higher raw signals of the relative luminescence units (RLU) in rows A and P and columns 1 and 24, resulting in a coefficient of variation (CV) of 18.97%. (**C, D, G**). By employing sealing membranes during the vehicle incubation period, edge effects were slightly reduced with a CV of 14.62%. (**E, G**) The use of the sealing membranes throughout the whole culture and treatment duration significantly reduced plate edge effects and showed spatial uniformity with a CV of 9.37%.

across all plates from 19% to 9% (**Fig. 2G**). Per the *Assay Guidance Manual*,[20] we assessed row and column drift for each of these plates. The largest difference between row means, as a percentage of the overall plate mean, was 59%, 29%, or 17%, in **Figures 2A**, **2C**, and **2E**, respectively. Similarly, the column drift results were 37%, 29%, and 15%. Employing sealing membranes throughout the complete assay period might affect the throughput; however, the optimized experimental conditions significantly reduced irregular spatial distribution and well-to-well variations.

Assay Validation of Organoid Cultures in 384-Well Format by Plate Uniformity Study

New high-throughput screening assays should be comprehensively validated for robustness of assay performance and pharmacologic relevance.[20] The plate uniformity study is required to assess uniformity and separation of the assay readout signals. We performed a plate uniformity study over three independent runs with six uniform signal plates for Max (maximum signal) and Min (minimum signal) signals and with six CRC plates (**Fig. 3**; **Suppl. Fig. S2**). The Max signal plates measured the maximum signal of the assay where the organoid cultures were treated with medium containing 0.25% DMSO (vehicle control). As a reference compound, we evaluated the broad-spectrum kinase inhibitor staurosporine and monitored the effects on organoid morphogenesis for 72 h using time-lapse microscopy (**Suppl. Movie**). We could demonstrate that staurosporine markedly affected organoid formation and integrity in a dose-dependent manner (**Suppl. Movie**). Thus, we selected staurosporine at 5 µM as the reference compound for the Min signal plates. For the CRC plates, the reference

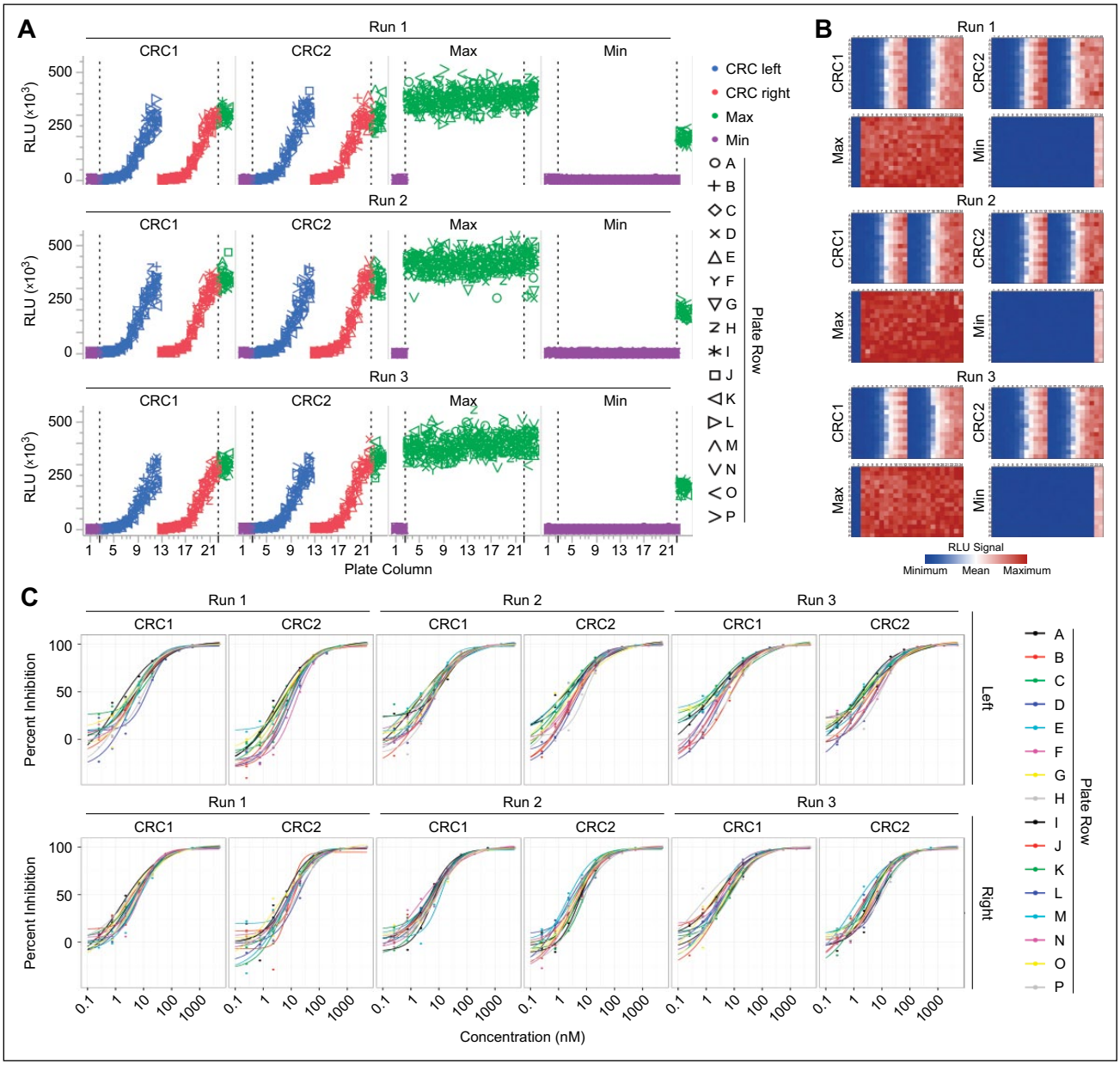

Figure 3. Assay validation by plate uniformity study. The plate uniformity study was carried out over three independent runs consisting of two concentration-response curve (CRC) plates (CRC1 and CRC2), one plate with the maximum signal (Max) and one plate with the minimum signal (Min) for each run for the patient-derived organoid sample 250-MW-P-TF-01-03. (**A, B**) The raw signals of the relative luminescence units (RLU) of all 12 plates were plotted against the respective plate column (**A**) and visualized by plate heat maps (**B**). (**C**) The four-parameter logistic CRCs were plotted for each side (left and right) of the CRC plates for all three runs, and each color represents a plate row.

compound was tested at 10 different dilutions (starting at 5 μM), resulting in 32 curves per plate in 384-well format (**Suppl. Fig. S2**). Inhibitor dose-dependent effects on cell viability were determined, and the RLU values were plotted with the well-level location (**Fig. 3A**) and visualized by plate heat maps (**Fig. 3B**). The corresponding four-parameter logistic CRCs were calculated and plotted for each plate row from left to right for each plate (**Fig. 3C**). The plate uniformity results were as follows. Maximum signal plate CVs were 5.1% to 12.2%, midpoint signal CVs were 8.5% to 12.4%, and minimum signal CVs were 11.0% to 15.6% (**Table 1**). These CVs all pass the 20% criterion. Plate Z' values were 0.62 to 0.83, and IC_{50} mean fold changes between plates were all acceptable at less than twofold (**Table 1**).[21] On the maximum signal plates, the row and column drift results of the maximum signal were less than 20% of the plate mean. On the minimum signal plates, the row and column drift results of the minimum signal were less than 50% of the plate mean. Because the minimum

Table 1. Results of the plate uniformity study.[a]

Patient Sample	Run	Plate	Type	Mean	SD	CV	SD MID %ACT	SW	Z′	Mean IC_{50}	Mean IC_{50} Fold Change
250-MW-P-TF-01-03	1	CRC1	Max	306,221	25,158	5.81		13.73	0.81	4.98 nM	1.50
			Min	6346	1059	11.80					
			6.86nM	142,318	17,123	8.51	5.71				
		CRC2	Max	296,801	51,152	12.19		4.98	0.62	7.48 nM	
			Min	6233	971	11.02					
			6.86nM	174,028	22,321	9.07	7.68				
		Max	Max	380,948	41,645	7.73		9.66	0.76		
			Min	5536	1205	15.40					
		Min	Max	196,052	14,949	5.39		14.87	0.82		
			Min	4918	1068	15.35					
	2	CRC1	Max	346,610	30,125	6.15		12.82	0.80	5.49 nM	1.73
			Min	6985	1255	12.70					
			6.86nM	169,806	22,617	9.42	6.66				
		CRC2	Max	338,845	44,077	9.20		7.59	0.71	3.18 nM	
			Min	6488	1019	11.10					
			6.86nM	146,339	23,900	11.55	7.19				
		Max	Max	420,684	46,008	7.73		9.72	0.76		
			Min	4718	1042	15.62					
		Min	Max	196,396	17,690	6.37		12.10	0.79		
			Min	5295	1029	13.75					
	3	CRC1	Max	299,714	26,911	6.35		12.38	0.80	3.65 nM	1.08
			Min	4975	938	13.33					
			6.86nM	128,070	22,441	12.39	7.61				
		CRC2	Max	325,594	34,338	7.46		10.01	0.76	3.94 nM	
			Min	7028	1314	13.22					
			6.86nM	140,559	24,659	12.41	7.74				
		Max	Max	395,775	45,538	8.14		9.02	0.75		
			Min	6030	1224	14.36					
		Min	Max	205,623	14,823	5.10		15.99	0.83		
			Min	4752	837	12.45					

[a]CRC, concentration-response curve; CV, coefficient of variation; Max, maximum signal; Min, minimum signal; SW, signal window; Z′, Z′ factor.
N = 352 for Max (Max plates) and Min (Min plates). *N* = 32 for Max (Min and CRC plates), Min (Max and CRC plates), and Mid (CRC plates).

raw signal mean was less than 2% of the maximum signal mean, this result is not a practical concern.

Assay Transition to Organoid Culture Strains Derived from Different Patients

Our results suggest that a novel assay platform for PD3D colon cancer organoid cultures could be established and validated in 384-well format. However, it is important to note that assay variations of different patient-derived culture strains could occur. For that reason, we aimed at evaluating additional organoid cultures from three different colon cancer patients (sample IDs 159-MB-P-TF-01-03, 327-MB-P-TF-01-03, and 364-CB-M-MF-01-04) by plate uniformity assessment (**Fig. 4A–D**). Given the complex and time-consuming expansion period to obtain sufficient material to perform a full plate uniformity study over three runs (i.e., 12× 384-well plates; **Suppl. Fig. S2**), we decided to assess a streamlined plate uniformity study over two independent runs with two uniform signal plates for Max signal and with two CRC plates (**Fig. 4A–D**; **Suppl. Fig. S3**). As performed for the full plate uniformity study (**Fig. 3**), RLU values were plotted with the well-level location (**Fig. 4A**) and visualized by plate heat maps for each patient-derived sample (**Fig. 4B**). The four-parameter logistic CRCs were plotted for each plate row from left to right for each CRC plate (**Fig. 4C**). The plate uniformity results were as follows. Maximum signal plate CVs were 3.6% to 6.5%, midpoint signal CVs were 8.3% to 17.0%, and minimum signal CVs were 10.6% to 29.7% (**Table 2**). These results were acceptable per the Assay Validation Guidelines,[20] which state that all CVs should be not greater than 20%, except for minimum signals, where the minimum signal SD is less than the mid and max signal SDs. Plate Z′ values were 0.8 to 0.89, and IC_{50} mean fold changes between plates were all acceptable at less than twofold (**Table 2**). On the maximum

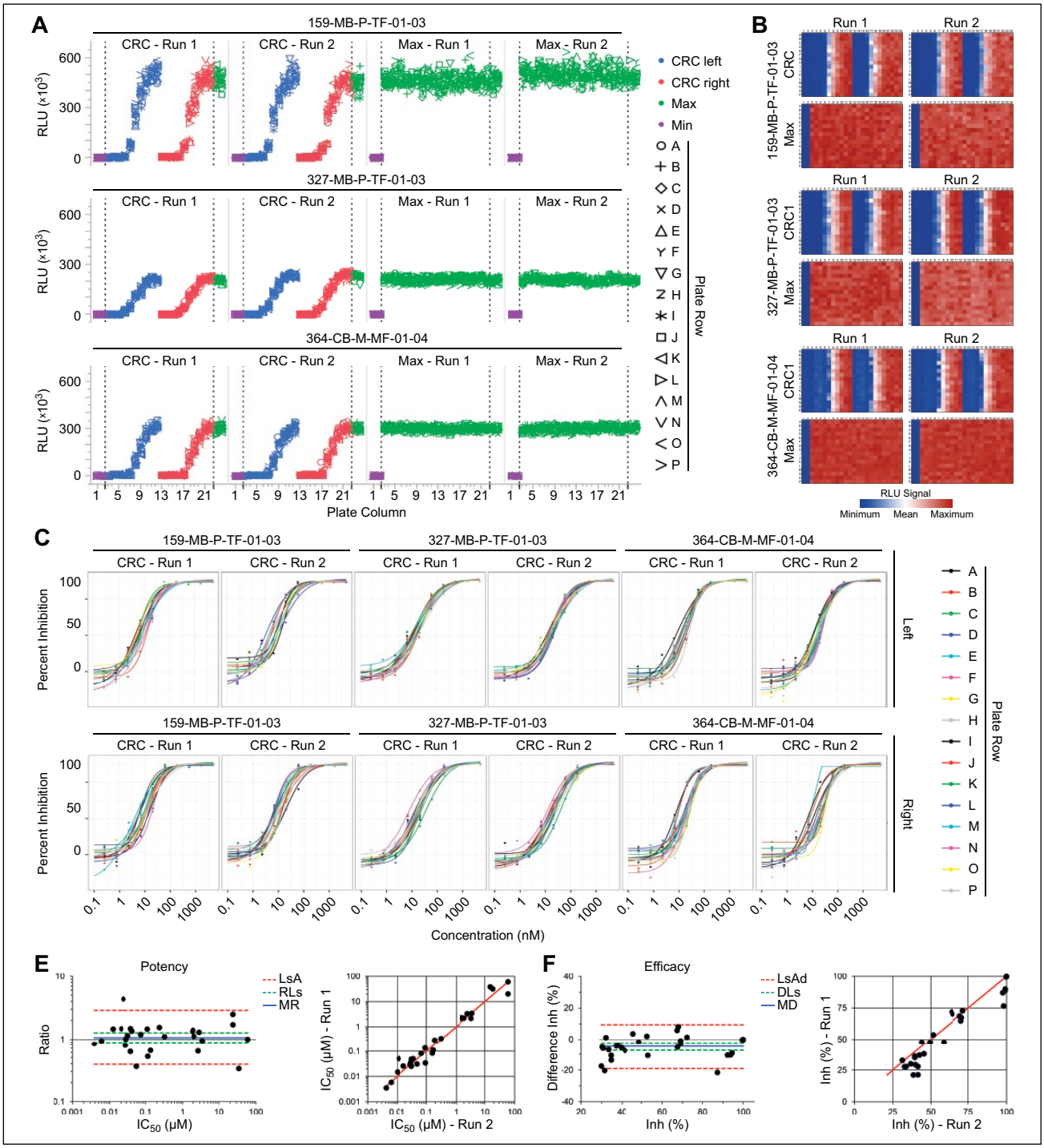

Figure 4. Streamlined plate uniformity study for different patient-derived samples and replicate-experiment study. (**A–C**) The streamlined plate uniformity study was carried out over two independent runs consisting of one concentration-response curve (CRC) plate and one plate with the maximum signal (Max) for each run. (**A, B**) The raw signals of the relative luminescence units (RLU) of all four plates for each patient-derived sample (159-MB-P-TF-01-03, 327-MB-P-TF-01-03, and 364-CB-M-MF-01-04) were plotted against the respective plate column (**A**) and visualized by plate heat maps (**B**). (**C**) The four-parameter logistic CRCs were plotted for each side (left and right) of the CRC plates for the two runs for the different patient-derived samples, and each color represents a plate row. (**E, F**) The replicate-experiment study was carried out for one patient-derived sample (159-MB-P-TF-01-03) consisting of two independent runs with the same set of compounds. The minimum significant ratio (MSR), limits of agreement (LsA) for potency estimates and the correlation of the IC_{50} values of both runs (**E**) as well as the minimum significant difference (MSD), limits of agreement for the difference (LsAd) for efficacy estimates, and the correlation of the maximum inhibition values of both runs (**F**) were calculated and visualized. The values for potency estimates were MSR = 2.72; LsA = 0.39 to 2.89; RLs = 0.89 to 1.27; MR = 1.06 (**E**). The values for efficacy estimates were MSD = 14.18; LsAd = −19.03 to 9.33; DLs = −7.41 to −2.30; MD = −4.85 (**F**). MD, mean difference; MR, mean ratio; DLs, difference limits (statistical limits of the mean difference); RLs, ratio limits (statistical limits of the mean ratio).

Table 2. Results of the streamlined plate uniformity studies for different patient-derived samples.

Patient Sample	Run	Plate	Type	Mean	SD	CV	SD MID %ACT	SW	Z′	Mean IC_{50}	Mean IC_{50} Fold Change
159-MB-P-TF-01-03	1	CRC	Max	472,661	39,724	5.94		13.77	0.82	18.09 nM	1.00
			Min	1035	223	15.22					
			20.58 nM	251,825	60,495	16.99	12.83				
	2	CRC	Max	449,423	41,071	6.46		12.43	0.80	18.18 nM	
			Min	889	204	16.20					
			20.58 nM	255,789	47,830	13.22	10.66				
	1	Max	Max	500,202	40,774	5.76		14.24	0.82		
			Min	1818	597	23.22					
	2	Max	Max	467,238	39,673	6.00		13.58	0.82		
			Min	1126	474	29.74					
327-MB-P-TF-01-03	1	CRC	Max	208,713	11,049	3.74		23.53	0.88	17.18 nM	1.17
			Min	855	291	24.06					
			20.58 nM	110,919	14,943	9.53	7.19				
	2	CRC	Max	231,340	15,167	4.64		18.44	0.86	20.16 nM	
			Min	879	223	17.96					
			20.58 nM	127,794	14,972	8.28	6.5				
	1	Max	Max	211,594	15,884	5.31		15.74	0.84		
			Min	681	186	19.26					
	2	Max	Max	208,034	13,988	4.75		17.94	0.86		
			Min	555	158	20.08					
364-CB-M-MF-01-04	1	CRC	Max	305,381	20,746	4.80		17.55	0.85	8.84 nM	1.16
			Min	3003	451	10.61					
			6.86 nM	181,713	32,355	12.59	10.7				
	2	CRC	Max	305,910	16,125	3.73		23.50	0.88	10.28 nM	
			Min	2731	491	12.72					
			6.86 nM	190,750	32,751	12.14	10.8				
	1	Max	Max	302,167	15,205	3.56		24.68	0.89		
			Min	3155	668	14.96					
	2	Max	Max	302,685	17,000	3.97		21.83	0.88		
			Min	3038	534	12.43					

CRC, concentration-response curve; CV, coefficient of variation; Max, maximum signal; Min, minimum signal; SW, signal window; Z′, Z′ factor. *N* = 352 for Max (Max plates). *N* = 32 for Max (CRC plates), Min (Max and CRC plates), and Mid (CRC plates).

signal plates, the row and column drift results of the maximum signal were less than 14% of the plate mean.

The next step in assay validation was to assess the reproducibility of the outcome measure, in this case the IC_{50} (potency) and maximum inhibition (efficacy; **Fig. 4E**, **F**). To illustrate this for one of the organoid models (sample ID 159-MB-P-TF-01-03), we tested 16 compounds in 10-point concentration-response format in two independent runs (**Suppl. Fig. S4**). IC_{50} values were obtained by fitting a four-parameter logistic curve to the data for each compound. For efficacy estimates, we calculated the minimum significant ratio (MSR),[22] limits of agreement (LsA), per the *Assay Guidance Manual*.[20] Accordingly, we determined the minimum significant difference (MSD) and limits of agreement for the difference (LsAd) for efficacy estimates. The MSR was 2.46, and the LsA were 0.46 to 2.77, which pass the criteria of MSR <3 and LsA within 0.33 to 3 (**Suppl. Fig. S4**). The MSD was 16.24 and the LsAd within −20.40 and 12.07 (**Suppl. Fig. S4**). Because the 16 compounds were tested in duplicates, the data were also analyzed as 32 separate curves. The results were similar, with MSR = 2.72 and LsA = 0.39 to 2.89 for potency estimates (**Fig. 4E**). In addition, the efficacy estimates were calculated with MSD = 14.18 and LsAd = −19.03 to 9.33 (**Fig. 4F**), indicative for passing all relevant criteria of the replicate-experiment study.[20]

Discussion

The application of 3D culture systems as disease-specific human drug-screening models has enormous potential to connect compound screening and clinical trials. Recent technical advances allow for engineering a cellular microenvironment that more closely mimics the physiological situation compared with conventional 2D cell cultures.[23–26] Primary organoid cultures with the property to self-organize and maintain the complexity of the tissue of origin are novel experimental patient-specific 3D model systems that could represent a new generation of drug-screening technology for pharmacogenomic

profiling.[15,16] A successful establishment of novel and complex technologies in the drug discovery pipeline requires implementation of automatic high-throughput platforms into the workflow as well as comprehensive assay validation studies.

Our results demonstrate that primary patient-derived tumor material can be used to establish a robust in vitro drug sensitivity assay. First, complex 3D structures are formed from single cells in miniaturized 384-well format with regular organoid morphogenesis. Our results are consistent with previous findings that single cells suspended into an extracellular matrix self-organize into luminized organoid structures.[9,13] We provide further experimental support for this concept for a 384-well–based assay system that is also applicable to drug-screening methodologies. Second, our approach allows for the use of robotic platforms for cell seeding and compound administration and thus facilitates high-throughput and reproducible screening studies. The high accuracy of the automatic platforms is particularly important in complex long-term 3D assays, as minor well-to-well differences might lead to significant readout variations. Third, we subjected the organoid drug sensitivity assay to systematic plate uniformity assessment and could validate the assay as a robust and reproducible high-throughput platform. After assay optimization, the patient-derived organoid platform passed all relevant validation criteria of assay performance and pharmacologic relevance.[20] Moreover, we introduced a streamlined plate uniformity study and demonstrated its validity for patient-derived colon cancer samples from different donors.

Despite the clear value of complex PD3D assays in high-throughput format, several challenges remain. It is conceivable that patient-derived samples from different tumor entities show diverse requirements for their establishment in 384-well format, and these different conditions must be taken into consideration when validating new assay platforms. Thus, it is recommended to perform a comprehensive plate uniformity study for each tumor tissue type established as a 3D organoid culture assay system and, as presented herein, subsequently apply a streamlined plate uniformity study for patient-specific samples derived from different donors from the respective tumor entity. Also, the requirement for a constant supply of fresh patient material would exclude their use as high-throughput platforms for large compound screens. However, the propagation of patient-derived tumor specimens has been recently reported for colon, pancreatic, and prostate tumors.[14,27,28] In addition, human pluripotent stem cells have been demonstrated as a source for colon, gastric, lung, and pancreatic organoid cultures.[11,12,29,30] For the development of novel patient tailoring strategies, a comprehensive correlation of compound response data with the genomic analysis is essential. Because of the complexity of multiple alterations in colorectal cancer[31] and consequently in PD3D organoid models, a large set of patient-derived organoid samples is critical to dissect a diverse response data set. Notably, Matano et al.[32] pioneered the use of the CRISPR-Cas9 (clustered regularly interspaced short palindromic repeats–CRISPR-associated 9) system in human intestinal organoids. With this technology, diverse oncogenic mutations could be engineered into organoids derived from normal colon.[32] Despite the experimental progress, to date, patient-derived organoid cultures do not mimic effects of the immune system, vascularization, and other effects of stromal elements. By increasing our understanding of the impact of the microenvironment on tumor progression, we may be able to generate predictive data from more biologically relevant experimental assays that incorporate multicellular constituents and physical properties of a tumor. Further investigation is required to establish sophisticated co-culture tumor models (e.g., with cancer-associated fibroblasts or endothelial cells[33–37]) as reproducible and standardized tools for translational research and drug discovery.

In summary, the study presented herein shows the establishment and validation of primary organoid cultures as an automated drug sensitivity platform. We anticipate that robust high-throughput technologies for patient-derived samples will be instrumental tools in the drug discovery pipeline as an invaluable link to disease-specific human models.

Acknowledgments

We gratefully acknowledge Jesús Castañon, José Luis Díaz-Puentes, Wenling Zhang, Bruna Calsina, Ana Hermoso, Ester Arroba, Julia Gutiérrez, Eduardo Goicoechea, and Laura Álvaro, from Eli Lilly and Company; Cathrin Davies and Yvonne Welte from Charité Universitätsmedizin Berlin, Germany; Caroline Schweiger from Medical University Graz; and Ulrich Keilholz from Charité Comprehensive Cancer Center for fruitful discussions and technical assistance. We thank Diego Megias and the CNIO Confocal Microscopy Unit for technical support.

Declaration of Conflicting Interests

The authors declared no potential conflicts of interest with respect to the research, authorship, and/or publication of this article.

Funding

The authors disclosed receipt of the following financial support for the research, authorship, and/or publication of this article: The research leading to these results has received support from the Innovative Medicines Initiative Joint Undertaking under grant agreement No. 115234 (OncoTrack), resources of which are composed of financial contribution from the European Union's Seventh Framework Programme (FP7/2007-2013) and EFPIA companies in kind contribution.

References

1. Garnett, M. J.; Edelman, E. J.; Heidorn, S. J.; et al. Systematic Identification of Genomic Markers of Drug Sensitivity in Cancer Cells. *Nature* **2012**, *483*, 570–575.
2. Griffith, L. G.; Swartz, M. A. Capturing Complex 3D Tissue Physiology In Vitro. *Nature Rev. Mol. Cell Biol.* **2006**, *7*, 211–224.
3. Sharma, S. V.; Haber, D. A.; Settleman, J. Cell Line-Based Platforms to Evaluate the Therapeutic Efficacy of Candidate Anticancer Agents. *Nat. Rev. Cancer* **2010**, *10*, 241–253.

4. Tentler, J. J.; Tan, A. C.; Weekes, C. D.; et al. Patient-Derived Tumour Xenografts as Models for Oncology Drug Development. *Nat. Rev. Clin. Oncol*. **2012**, *9*, 338–350.
5. Hidalgo, M.; Bruckheimer, E.; Rajeshkumar, N. V.; et al. A Pilot Clinical Study of Treatment Guided by Personalized Tumor Grafts in Patients with Advanced Cancer. *Mol. Cancer Ther*. **2011**, *10*, 1311–1316.
6. Yamada, K. M.; Cukierman, E. Modeling Tissue Morphogenesis and Cancer in 3D. *Cell* **2007**, *130*, 601–610.
7. Hoffmann, J. Integrative Oncology Drug Discovery Accompanied by Preclinical Translational Research as Prerequisite for Clinical Development. *Chinese Clin. Oncol*. **2014**, *3*, 15.
8. Kijanska, M.; Kelm, J. In Vitro 3D Spheroids and Microtissues: ATP-Based Cell Viability and Toxicity Assays. In *Assay Guidance Manual*; Sittampalam, G. S.; Coussens, N. P.; Nelson, H.; et al., Eds.; Eli Lilly & Company and the National Center for Advancing Translational Sciences: Bethesda (MD), **2004**.
9. Sato, T.; Vries, R. G.; Snippert, H. J.; et al. Single Lgr5 Stem Cells Build Crypt-Villus Structures In Vitro without a Mesenchymal Niche. *Nature* **2009**, *459*, 262–265.
10. Sato, T.; Stange, D. E.; Ferrante, M.; et al. Long-Term Expansion of Epithelial Organoids from Human Colon, Adenoma, Adenocarcinoma, and Barrett's Epithelium. *Gastroenterology* **2011**, *141*, 1762–1772.
11. Huang, L.; Holtzinger, A.; Jagan, I.; et al. Ductal Pancreatic Cancer Modeling and Drug Screening Using Human Pluripotent Stem Cell- and Patient-Derived Tumor Organoids. *Nat. Med*. **2015**, *21*, 1364–1371.
12. McCracken, K. W.; Cata, E. M.; Crawford, C. M.; et al. Modelling Human Development and Disease in Pluripotent Stem-Cell-Derived Gastric Organoids. *Nature* **2014**, *516*, 400–404.
13. Drost, J.; Karthaus, W. R.; Gao, D.; et al. Organoid Culture Systems for Prostate Epithelial and Cancer Tissue. *Nat. Protoc*. **2016**, *11*, 347–358.
14. van de Wetering, M.; Francies, H. E.; Francis, J. M.; et al. Prospective Derivation of a Living Organoid Biobank of Colorectal Cancer Patients. *Cell* **2015**, *161*, 933–945.
15. Sachs, N.; Clevers, H. Organoid Cultures for the Analysis of Cancer Phenotypes. *Curr. Opin. Genet. Dev*. **2014**, *24*, 68–73.
16. Ranga, A.; Gjorevski, N.; Lutolf, M. P. Drug Discovery through Stem Cell-Based Organoid Models. *Adv. Drug Deliv. Rev*. **2014**, 69–70, 19–28.
17. Kondo, J.; Endo, H.; Okuyama, H.; et al. Retaining Cell-Cell Contact Enables Preparation and Culture of Spheroids Composed of Pure Primary Cancer Cells from Colorectal Cancer. *Proc. Natl. Acad. Sci. U.S.A*. **2011**, *108*, 6235–6240.
18. Kevorkov, D.; Makarenkov, V. Statistical Analysis of Systematic Errors in High-Throughput Screening. *J. Biomol. Screen*. **2005**, *10*, 557–567.
19. Lundholt, B. K.; Scudder, K. M.; Pagliaro, L. A Simple Technique for Reducing Edge Effect in Cell-Based Assays. *J. Biomol. Screen*. **2003**, *8*, 566–570.
20. Iversen, P. W.; Beck, B.; Chen, Y. F.; et al. HTS Assay Validation. In *Assay Guidance Manual*; Sittampalam, G. S.; Coussens, N. P.; Nelson, H.; et al., Eds.; Eli Lilly & Company and the National Center for Advancing Translational Sciences: Bethesda (MD), **2004**.
21. Iversen, P. W.; Eastwood, B. J.; Sittampalam, G. S.; et al. A Comparison of Assay Performance Measures in Screening Assays: Signal Window, Z′ Factor, and Assay Variability Ratio. *J. Biomol. Screen*. **2006**, *11*, 247–252.
22. Haas, J. V.; Eastwood, B. J.; Iversen, P. W.; et al. Minimum Significant Ratio: A Statistic to Assess Assay Variability. In *Assay Guidance Manual*; Sittampalam, G. S.; Coussens, N. P.; Nelson, H.; et al., Eds.; Eli Lilly & Company and the National Center for Advancing Translational Sciences: Bethesda (MD), **2004**.
23. Lee, G. Y.; Kenny, P. A.; Lee, E. H.; et al. Three-Dimensional Culture Models of Normal and Malignant Breast Epithelial Cells. *Nat. Methods* **2007**, *4*, 359–365.
24. Boehnke, K.; Mirancea, N.; Pavesio, A.; et al. Effects of Fibroblasts and Microenvironment on Epidermal Regeneration and Tissue Function in Long-Term Skin Equivalents. *Eur. J. Cell Biol*. **2007**, *86*, 731–746.
25. Friedrich, J.; Seidel, C.; Ebner, R.; et al. Spheroid-Based Drug Screen: Considerations and Practical Approach. *Nat. Protoc*. **2009**, *4*, 309–324.
26. Beachley, V. Z.; Wolf, M. T.; Sadtler, K.; et al. Tissue Matrix Arrays for High-Throughput Screening and Systems Analysis of Cell Function. *Nat. Methods* **2015**, *12*, 1197–1204.
27. Boj, S. F.; Hwang, C. I.; Baker, L. A.; et al. Organoid Models of Human and Mouse Ductal Pancreatic Cancer. *Cell* **2015**, *160*, 324–338.
28. Gao, D.; Vela, I.; Sboner, A.; et al. Organoid Cultures Derived from Patients with Advanced Prostate Cancer. *Cell* **2014**, *159*, 176–187.
29. Dye, B. R.; Hill, D. R.; Ferguson, M. A.; et al. In Vitro Generation of Human Pluripotent Stem Cell Derived Lung Organoids. *eLife* **2015**, *4*.
30. Spence, J. R.; Mayhew, C. N.; Rankin, S. A.; et al. Directed Differentiation of Human Pluripotent Stem Cells into Intestinal Tissue In Vitro. *Nature* **2011**, *470*, 105–109.
31. Sjoblom, T.; Jones, S.; Wood, L. D.; et al. The Consensus Coding Sequences of Human Breast and Colorectal Cancers. *Science* **2006**, *314*, 268–274.
32. Matano, M.; Date, S.; Shimokawa, M.; et al. Modeling Colorectal Cancer Using CRISPR-Cas9-Mediated Engineering of Human Intestinal Organoids. *Nat. Med*. **2015**, *21*, 256–262.
33. Dolznig, H.; Rupp, C.; Puri, C.; et al. Modeling Colon Adenocarcinomas In Vitro: A 3D Co-Culture System Induces Cancer-Relevant Pathways upon Tumor Cell and Stromal Fibroblast Interaction. *Am. J. Pathol*. **2011**, *179*, 487–501.
34. Thoma, C. R.; Stroebel, S.; Rosch, N.; et al. A High-Throughput-Compatible 3D Microtissue Co-Culture System for Phenotypic RNAi Screening Applications. *J. Biomol. Screen*. **2013**, *18*, 1330–1337.
35. Takebe, T.; Sekine, K.; Enomura, M.; et al. Vascularized and Functional Human Liver from an iPSC-Derived Organ Bud Transplant. *Nature* **2013**, *499*, 481–484.
36. Pinto, S.; Schmidt, K.; Egle, S.; et al. An Organotypic Coculture Model Supporting Proliferation and Differentiation of Medullary Thymic Epithelial Cells and Promiscuous Gene Expression. *J. Immunol*. **2013**, *190*, 1085–1093.
37. Linde, N.; Gutschalk, C. M.; Hoffmann, C.; et al. Integrating Macrophages into Organotypic Co-Cultures: A 3D In Vitro Model to Study Tumor-Associated Macrophages. *PloS One* **2012**, *7*, e40058.